Biomedical Optics EXPRESS

Light scattering from edematous human corneal grafts' microstructure: experimental study and electromagnetic modelization

Olivier Casadessus,[1,*] Gaëlle Georges,[1] Laure Siozade Lamoine,[1] Carole Deumié,[1] and Louis Hoffart[2]

[1]*Institut Fresnel, UMR CNRS 7249, Université d'Aix-Marseille, Ecole Centrale Marseille, Domaine universitaire de Saint Jérôme, Avenue Escadrille Normandie Niemen, 13 397 Marseille cedex 20, France*
[2]*Service d'Ophtalmologie de l'Hôpital de la Timone, APHM, Université d'Aix-Marseille, 264 rue Saint Pierre, 13 385 Marseille Cedex 5, France*
**olivier.casadessus@fresnel.fr*

Abstract: Along with the lens, the cornea is the only transparent tissue in the human body. However, the development of an edema involves structural disturbances increasing light scattering and leading to the opacification of the cornea. Several mechanisms of transparency loss have been studied in the literature, but the whole phenomenon is complex and the part played by each scatterer is still unclear. We propose here to study human corneal grafts combining microscopic OCT imagery with far-field measurement of the scattered light in the reflected half-space. We introduce afterwards numerical calculations based on electromagnetic equations solved with first order approximation to link the observed microscopic-scale structural modifications with the intensity level of the scattered light, and to try and quantify the relationship between them.

OCIS codes: (170.4500) Optical coherence tomography; (290.5820) Scattering measurements; (000.2190) Experimental physics; (170.4470) Ophthalmology; (170.6935) Tissue characterization.

References and links

1. T. Nishida, "Cornea: anatomy and physiology," in *Cornea: Fundamentals, Diagnosis and Management*, 2nd ed., J. H. Krachmer, M. J. Mannis, and E. J. Holland, eds. (Elsevier/Mosby, 2005).
2. D. M. Maurice, "The structure and transparency of the cornea," J. Physiol. **136**(2), 263–286 (1957).
3. R. W. Hart and R. A. Farrell, "Light scattering in the cornea," J. Opt. Soc. Am. **59**(6), 766–774 (1969).
4. G. B. Benedek, "Theory of transparency of the eye," Appl. Opt. **10**(3), 459–473 (1971).
5. J. N. Goldman, G. B. Benedek, C. H. Dohlman, and B. Kravitt, "Structural alterations affecting transparency in swollen human corneas," Invest. Ophthalmol. **7**(5), 501–519 (1968).
6. R. A. Farrell, R. L. McCally, and P. E. R. Tatham, "Wave-length dependencies of light scattering in normal and cold swollen rabbit corneas and their structural implications," J. Physiol. **233**(3), 589–612 (1973).
7. D. A. Peyrot, F. Aptel, C. Crotti, F. Deloison, S. Lemaire, T. Marciano, S. Bancelin, F. Alahyane, L. Kowalczuk, M. Savoldelli, J.-M. Legeais, and K. Plamann, "Effect of incident light wavelength and corneal edema on light scattering and penetration: laboratory study of human corneas," J. Refract. Surg. **26**(10), 786–795 (2010).
8. J. V. Jester, T. Møller-Pedersen, J. Huang, C. M. Sax, W. T. Kays, H. D. Cavangh, W. M. Petroll, and J. Piatigorsky, "The cellular basis of corneal transparency: evidence for 'corneal crystallins'," J. Cell Sci. **112**(Pt 5), 613–622 (1999).
9. T. Møller-Pedersen, "Keratocyte reflectivity and corneal haze," Exp. Eye Res. **78**(3), 553–560 (2004).
10. E. Pels, H. Beele, and I. Claerhout, "Eye bank issues: II. Preservation techniques: warm versus cold storage," Int. Ophthalmol. **28**(3), 155–163 (2008).
11. A. H. Wolf, U. C. Welge-Lüßen, S. Priglinger, D. Kook, M. Grueterich, K. Hartmann, A. Kampik, and A. S. Neubauer, "Optimizing the deswelling process of organ-cultured corneas," Cornea **28**(5), 524–529 (2009).
12. D. Huang, E. A. Swanson, C. P. Lin, J. S. Schuman, W. G. Stinson, W. Chang, M. R. Hee, T. Flotte, K. Gregory, C. A. Puliafito, and J. G. Fujimoto, "Optical coherence tomography," Science **254**(5035), 1178–1181 (1991).
13. E. Beaurepaire, A. C. Boccara, M. Lebec, L. Blanchot, and H. Saint-Jalmes, "Full-field optical coherence microscopy," Opt. Lett. **23**(4), 244–246 (1998).

#163673 - $15.00 USD Received 27 Feb 2012; revised 31 Mar 2012; accepted 29 Apr 2012; published 2 Jul 2012

14. A. Dubois, L. Vabre, A. C. Boccara, and E. Beaurepaire, "High-resolution full-field optical coherence tomography with a Linnik microscope," Appl. Opt. **41**(4), 805–812 (2002).
15. G. Latour, G. Georges, L. S. Lamoine, C. Deumié, J. Conrath, and L. Hoffart, "Human graft cornea and laser incisions imaging with micrometer scale resolution full-field optical coherence tomography," J. Biomed. Opt. **15**(5), 056006 (2010).
16. C. Amra, D. Torricini, and P. Roche, "Multiwavelength (0.45-10.6 μm) angle-resolved scatterometer or how to extend the optical window," Appl. Opt. **32**(28), 5462–5474 (1993).
17. G. Latour, G. Georges, L. Siozade-Lamoine, C. Deumié, J. Conrath, and L. Hoffart, "Light scattering from human corneal grafts: Bulk and surface contribution," J. Appl. Phys. **108**(5), 053104 (2010).
18. C. Amra, C. Grèzes-Besset, and L. Bruel, "Comparison of surface and bulk scattering in optical multilayers," Appl. Opt. **32**(28), 5492–5503 (1993).
19. C. Amra, "First-order vector theory of bulk scattering in optical multilayers," J. Opt. Soc. Am. A **10**(2), 365–374 (1993).
20. M. Born and E. Wolf, *Principle of Optics*, 6th ed. (Pergamon, New York, 1986), p.453.
21. C. Deumié, R. Richier, P. Dumas, and C. Amra, "Multiscale roughness in optical multilayers: atomic force microscopy and light scattering," Appl. Opt. **35**(28), 5583–5594 (1996).
22. S. Patel, J. Marshall, and F. W. Fitzke III, "Refractive index of the human corneal epithelium and stroma," J. Refract. Surg. **11**(2), 100–105 (1995).
23. K. M. Meek, D. W. Leonard, C. J. Connon, S. Dennis, and S. Khan, "Transparency, swelling and scarring in the corneal stroma," Eye (Lond.) **17**(8), 927–936 (2003).
24. E. Popov and M. Nevière, "Maxwell equations in Fourier space: fast-converging formulation for diffraction by arbitrary shaped, periodic, anisotropic media," J. Opt. Soc. Am. A **18**(11), 2886–2894 (2001).
25. L. Arnaud, G. Georges, J. Sorrentini, M. Zerrad, C. Deumié, and C. Amra, "An enhanced contrast to detect bulk objects under arbitrary rough surfaces," Opt. Express **17**(7), 5758–5773 (2009).

1. Introduction

Along with the crystalline lens, the cornea is the only transparent tissue in the human body. This stiff part of the eye, an outer layer allowing the transmission of the light to the retina with a 90% transmission factor over the visible spectrum, is indeed not vascularized, thereby avoiding hemoglobin-induced light absorption, and presents a very particular structure, the stability of which is necessary to preserve its transparency.

In physiological conditions, the corneal disc is 11 mm wide and 530 μm thick in average. Its common description is that it consists in the juxtaposition of 5 layers (Fig. 1) [1].

The epithelium and endothelium are the outermost layers, respectively on the tear film side (external part of the eye) and the aqueous side (internal part of the eye). The epithelium is composed of 5 to 6 rows of cells. Together with the tear film, it ensures the smoothness of the corneal surface. Additionally to a protective role against external aggressions, it contributes to nourishing the tissue, taking nutrients and oxygen from the tears. The endothelium is a 8μm-thick cell monolayer whose main role is to act as an osmotic pump: this, additionally to minor vaporization occurring from the epithelium side, ensures the cornea to regulate its thickness and avoiding swelling because of a too high hydration.

The second couple of layers includes the Bowman's and the Descemet's membranes, respectively in contact with the epithelium and the endothelium. These acellular layers are principally made of randomly disposed collagen fibrils over a thickness of 10 μm, and contribute to the structure and protection of the central part of the cornea: the stroma.

This last layer represents 90% of the total thickness of the cornea, and its structure is responsible for the tissue's transparency. As a layer, the stroma is composed of about 300 piled-up 2 μm-thick lamellas. These lamellas are composed of highly uniform collagen fibrils, with a mean diameter of 31 nm, spaced homogeneously with a 62 nm step, and aligned the one to the others [2]. Studies focusing on such a particular structure enlightened a phase destructive phenomenon canceling the individual scattering behavior of the fibrils, and inducing the light to be transmitted along the propagation direction, as long as the regular fibrillar lattice is maintained at least at short-term range [2–4]. Those fibrils are regularly renewed by keratocytes, flat cells with a stellar shape, up to 50 μm large and 1 μm thick on average, counting for up to 17% of the total volume of the stroma.

Disturbances in the general equilibrium of the cornea such as mechanical strains or hydration troubles may lead to tissue clouding. Edema is a manifestation of such disturbances,

#163673 - $15.00 USD Received 27 Feb 2012; revised 31 Mar 2012; accepted 29 Apr 2012; published 2 Jul 2012

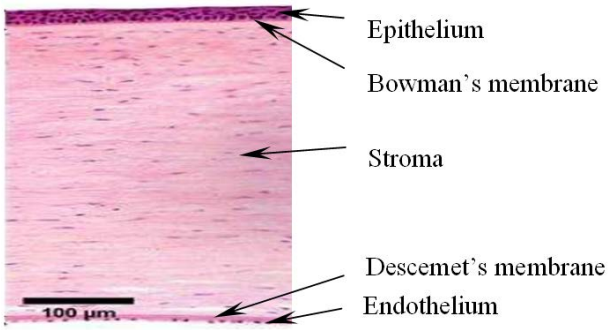

Fig. 1. Histological section of a human cornea (source: www.missionforvisionusa.org).

and may be consecutive to a wound or an endothelial dysfunction, causing haziness in the cornea. Because of a too high hydration level, the tissue tends to swell, disorganizing the fibrillar structure of the stroma. The required short-term order to ensure transparency is broken and fibril-free spaces appear within the lamellas as noticed by Goldman et al., electron micrography revealing the presence of the so-called "lakes" [5]. Therefore, structural defects intervene at different scales, involving in particular nanometric perturbations in the regular fibrillar lattice and the apparition of large fibril-free areas up to several micrometers large. Multiwavelength modeling and experimental studies highlighted different behaviors following the degree of edema [4,6,7]: the wavelength dependence of the scattered light's intensity is coherent with a major contribution of the fibrillar structure at physiological state (Rayleigh scattering), and with a larger structures' contribution predominance when the cornea swells (Mie scattering). In addition, other studies pointed out an increase in scattering because of keratocytes, due to a deficiency of the proteins which normally ensure the homogenization of the local refractive index [8,9]. However, the loss of transparency is a complex phenomenon which involves different spatial-scaled perturbations, and the role of each potential scatterer remains unclear.

The goal of this paper is to propose a study of the cornea at a micrometric scale during edema development, combining imagery and scattering measurements to follow the evolution of internal structures when the cornea swells, and relate it with its transparency. As aforementioned, studies [4,6,7] pointed out a major Mie scattering-like contribution when the cornea reaches non-physiologic thicknesses. This study focuses on scattering differences due to internal structures whose dimensions are superior to one micrometer. After a purely experimental approach, we use an electromagnetic model adapted for low-scattering media in an attempt to numerically link microstructure and scattering. The idea is to observe how the structural organization influences the scattering behavior of the tissue, but also to try and quantify this behavior for corneal graft sorting purposes and to prepare in-vivo diagnosis in the future.

2. Experimental investigations

This part is dedicated to an experimental study of human corneal grafts. As mentioned previously, we aim to follow the microstructural and scattering properties' evolutions of samples with their degree of edema. We had a particular interest in the backscattered field and in the development of the "lakes" within edematous corneas.

2.1 Samples

We obtained 13 human corneal grafts rejected from the tissue bank of Marseille (Etablissement Français du Sang Alpes-Méditerranée, Marseille, France) due to physiological issues (detected opacity, low endothelial cells density…). The grafts were stored in CorneaMax® (Eurobio, France) at ambient temperature. The samples had a thickness more

#163673 - $15.00 USD Received 27 Feb 2012; revised 31 Mar 2012; accepted 29 Apr 2012; published 2 Jul 2012

important than in *in vivo* conditions: this was due to the conservation technique that induced the graft to swell (see [10] for more details about organ culture preservation technique).

To study several edema degrees, different grafts were submitted to refrigeration or osmotic solution baths (amylum based solution Voluven® (Fresenius Kabi, France)— the effect on corneal graft for another colloid (Dextran) is presented in [11]). All the observations were realized during an average period of one week after receiving the tissue in our laboratory. The samples were immersed in a tank filled with balanced salt solution (BSS) to prevent them from dehydrating during the experiments.

2.2 Experimental setups

2.2.1 Imaging technique

Optical coherence tomography [12] was chosen to image the structure of the cornea. This technique based on low-coherence interferometry allows three-dimensional imagery and is nowadays commonly used for clinical eye investigation.

A full-field optical coherence tomography setup (temporal domain) based on the Linnik interferometer configuration [13,14] was developed (Fig. 2). We obtained images with a micrometric resolution in all three directions of space [15]. The observation area is a 250x190 μm^2 window covering the center of the tissue. The z-scan along the thickness is operated using a piezoelectric stage with a range up to 3 mm, so the tissue can be scanned on its whole depth (from 550 to 1200 µm for the studied samples). With water immersion objectives, the sensitivity was estimated over 80 dB with a 200-frame accumulation. Each sample was scanned at a pace of 2.5 seconds/image.

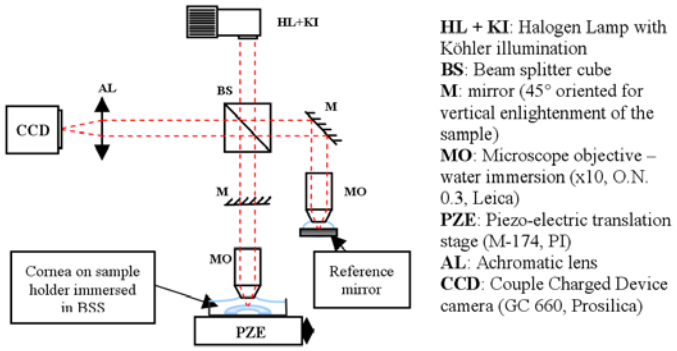

Fig. 2. Full-field optical coherence tomography configuration.

2.2.2 Scattering measuring device

Additionally, angular-resolved scattered light intensity measurements [16] were operated. The sample was illuminated at normal incidence on its center using a HeNe laser (632.8 nm), and a detector placed on a rotating arm was able to perform a 360° measurement of the scattering intensity. The sample was probed by the light whose interaction with the structures it met (surface defects or bulk heterogeneities) within the illumination surface (1mm-wide spot) resulted in scattering phenomena.

Due to the scattered light repartition, only the incident plane was considered to characterize the samples. For this study, we focused on the reflected half-space (angles between 0 and 90° where 0 is the sample's normal direction, but only the angular range from 6 to 70° is relevant because of the detector's and the sample holder's masking). This experimental configuration in the reflected half-space was chosen because it is the only space accessible in view of achieving *in vivo* characterization in the future. The dynamics of the experiment, delimited by the intensity levels measured using a lambertian and without any sample, was of 6 decades (Fig. 3).

#163673 - $15.00 USD Received 27 Feb 2012; revised 31 Mar 2012; accepted 29 Apr 2012; published 2 Jul 2012

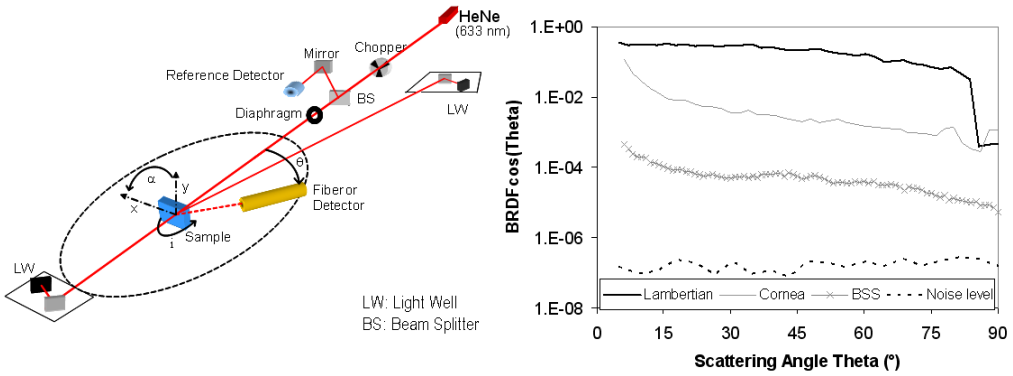

Fig. 3. Angular-resolved scattering measuring setup scheme (left) and intensity levels for a cornea and BSS with dynamics measurements (right).

The use of those two setups provides a non-contact and non-invasive characterization of the tissue, with on the one hand microscopic repartition of inhomogeneities and on the other hand a global response of the sample, through the measurement of the light scattered by all the graft's structures being probed by the illumination's wavelength.

2.3 Micrometric-scale structural evolutions

For each sample, optical coherence tomography was used to evaluate the corneal thickness and to image its microscopic structure evolution with swelling.

The setup is able to highlight the different layers of the cornea, and the differences of homogeneity they present can be observed [15]. Especially, we noticed the homogeneous aspect of the Bowman's and Descemet's membranes. However, we had a particular interest in the stroma whose structure presents significant variations following the degree of edema in comparison with the other layers.

For thin preserved donor corneas (thickness between 500 and 700 µm), OCT scans revealed a homogenous medium with keratocytes included all along the stroma (Fig. 4). We observed on these images the presence of the epithelial layer, but epithelium was most of the time degraded or absent when received in our laboratory, certainly due to too frequent manipulations or important storage periods in the tissue bank. Nevertheless, for thin grafts, no significant change in the structure of the other layers was observed that could be attributed to the presence or absence of the epithelium.

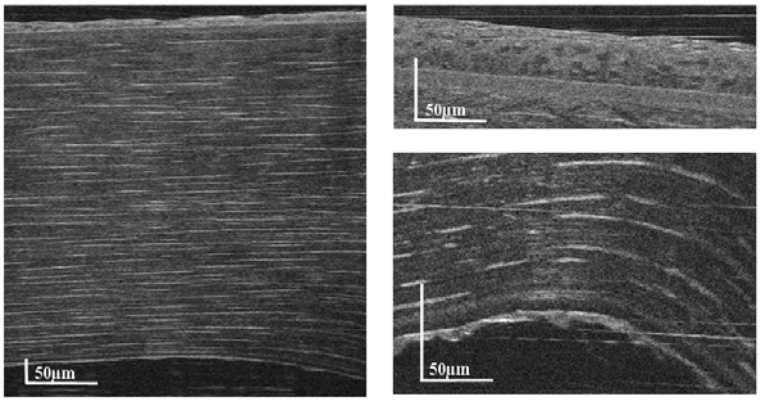

Fig. 4. OCT images from a 670 µm-thick cornea; depth-scan along the whole depth (left) and details of the anterior part with epithelium and Bowman's membrane (upper right) and the posterior part with stroma, Descemet's layer and endothelium (lower right).

#163673 - $15.00 USD Received 27 Feb 2012; revised 31 Mar 2012; accepted 29 Apr 2012; published 2 Jul 2012

When the cornea swells, variations are observed in the stroma. Liquid infiltrations ("lakes") appear as darker areas within the stroma. When observing one graft in particular, those lakes develop first from the endothelium side and their extension within the tissue rises with the thickness and edematous state of the cornea. Such evolution is illustrated in Fig. 5 where lamellar gaps extend while the tissue swells.

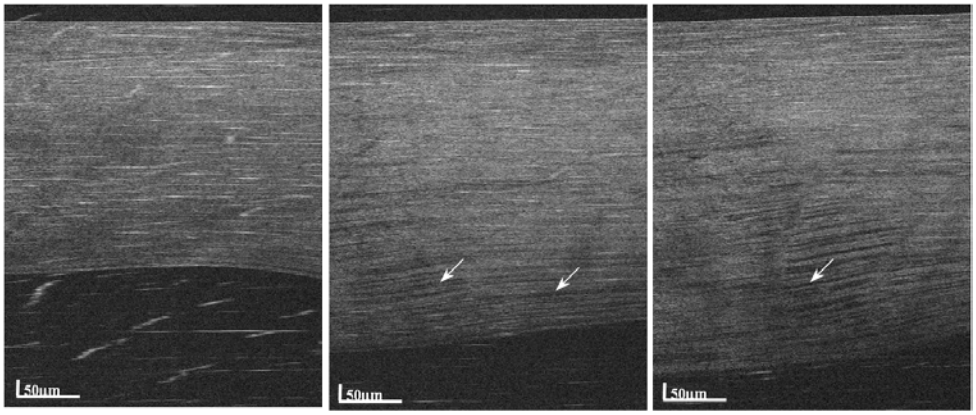

Fig. 5. Depth-scan OCT slices for one cornea at three different edematous states; thicknesses are from left to right of 730, 795 and 815 µm; arrows point out lakes appearing when the corneal swells.

We observed a systematic presence of lakes in all the samples whose thickness was over 800 µm. However, the size and density of those lakes varied from one cornea to another and had no obvious relation with the thickness or the relative expansion (calculated as the ratio between the thickness of one sample and its initial thickness when received in our laboratory). Moreover, additionally to the long and thin infiltrations due to lamellar separation, we noticed the presence of shorter and thicker lakes sparsely distributed in the stroma. Therefore two general lake distributions were visible depending on the graft studied: wide lamellar interspaces (over 100 µm in a plan parallel to the surface of the cornea) with an important density, or limited-sized lakes (up to 50 µm) sparsely disposed (Fig. 6). Each graft presented preferentially one or the other type of distribution and no connection with the thickness could be established.

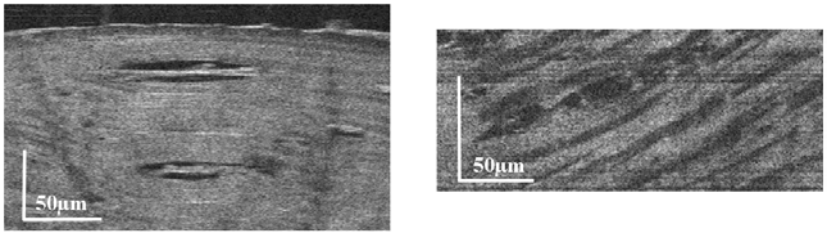

Fig. 6. Lakes details: short and thick lakes (left) and elongated liquid infiltrations (right).

2.4 Scattering intensity measurements

Scattered light intensity was measured for each corneal graft (preliminary measurements were presented in [17]). This was preceded and followed by a thickness evaluation using the OCT setup, in order to take into account the dynamic of the cornea whose thickness may evolve over the duration of the entire characterization process (approximately an hour and a half for scattering measurement and OCT imaging). The thickness related to the light scattering measurement was then evaluated with a ±25 µm precision.

#163673 - $15.00 USD Received 27 Feb 2012; revised 31 Mar 2012; accepted 29 Apr 2012; published 2 Jul 2012

Figure 7(a) presents angular-resolved intensity levels related to different thicknesses for one sample after being treated to modify its hydration state. The intensity level increases with the thickness, here directly related to the hydration rate of the cornea.

Figure 7(b) represents the same scattering measurements done for a whole series of corneas, including tissues submitted to the thickness variation protocol. We observed again a general increase of the scattering level with the thickness of the graft. While the curves aspect is rather similar for large angles, we notice disparities for low angles (typically inferior to 20°). As already mentioned in [17], while a major bulk scattering influence is expected for high angles, surface roughness and bulk effect may be more difficult to discriminate for lower angles. As we studied here different samples, their surfaces were likely to vary from one graft to another following the manipulations they were submitted to. Moreover, experimental configuration artifacts may have intervened, such as the quality of cleanness of the tank in which they were immersed. Consequently, only angles beyond 20° were taken into account from then on.

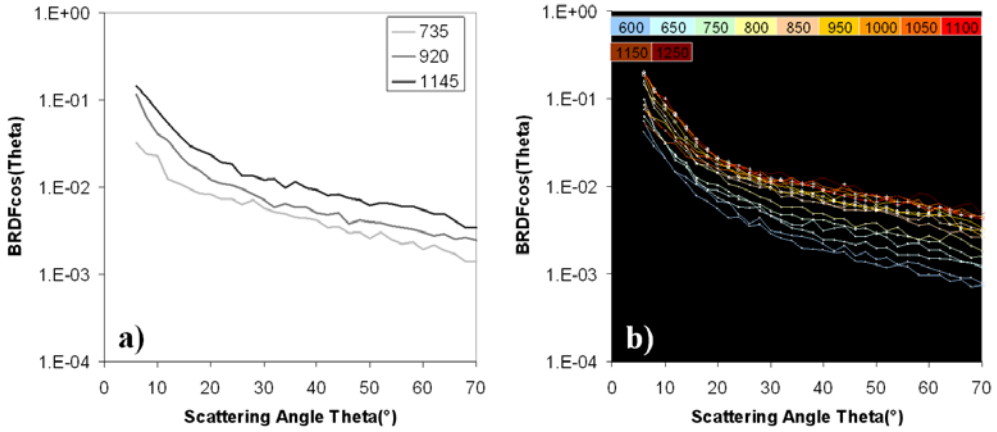

Fig. 7. Angular-resolved measurement in the reflected half-space for corneas at different edematous states. Intensity levels are plotted for one unique cornea at different hydration states after swelling and deswelling protocols (left). Same measurements are executed for different grafts with color indications referring to the thickness of the sample (right).

We then introduced another parameter, directly calculated from the intensity angular measurement: the Total Integrated Scattering (TIS). TIS represents the global scattering behavior of the graft, and is calculated as follows:

$$TIS = \iint_{\theta,\varphi} I(\theta,\varphi)\sin(\theta)\,d\theta d\varphi$$

with (θ,φ) the polar coordinates of the locally measured point. In order to select only the relevant portion of the curve, the angular range of interest was limited to angles between 20 and 70° in the incidence plane (φ = 0°).

As for an *in vivo* study, we don't have access to transmission values for the quantification of the graft's transparency. Nonetheless, the comparison of the TIS defined above with macroscopic pictures of the grafts showed clearly that its evolution was coherent with the transparency degree of the sample (Fig. 8). From then on, scattering results were thus evaluated in term of TIS in the reflective half-space, which appeared as a convenient parameter to represent the transparency state of the grafts.

Plotting the TIS values as a function of thickness (Fig. 9) revealed their global joint evolution. Besides, we observed this relationship was not so simple, with fluctuations, in particular when the thickness reached 800 µm.

#163673 - $15.00 USD Received 27 Feb 2012; revised 31 Mar 2012; accepted 29 Apr 2012; published 2 Jul 2012

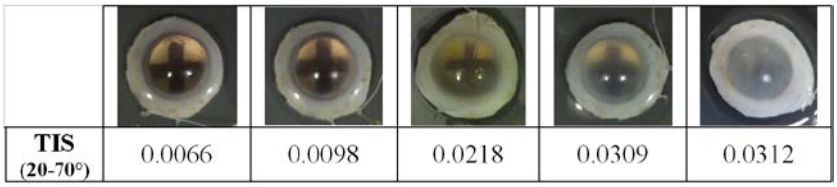

Fig. 8. Comparison of visual impression and TIS parameter. Corneal grafts are laid on a cross pattern to help appreciate the transparency and the associated TIS values are calculated for scattering angles between 20 and 70°.

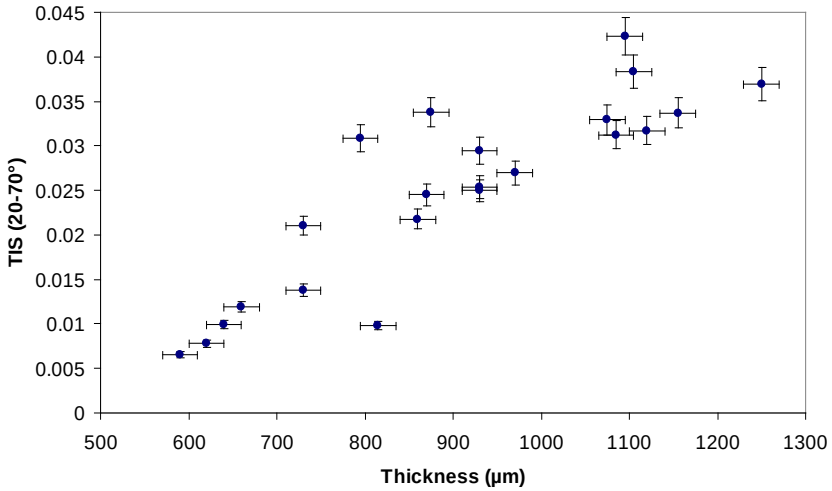

Fig. 9. Total Integrated Scattering calculated in the reflected half-space as a function of the thickness measured with OCT.

2.5 Structure and scattering

When considering the samples globally, the analysis of scattering intensity measurements jointly with OCT imagery did not reveal any simple correlation between structure and scattering intensity level.

Studying the case of one particular graft usually led to observations that were in accordance with the intuitively expected behavior: when the cornea swells, the TIS value increases, as does the density of the lakes within the stroma. But an extension to the comparison of several tissues did not reveal a particular structure specific to a particular scattering level. Of course each cornea possesses its own physiologic behavior, relatively to the state of their respective endothelial pump and general quality of the tissue itself, and this fact may enlighten the observed disparities.

Nonetheless, some structural trends could be noticed, such as a generally deeper lakes' penetration when the cornea presents a high TIS, and, for a given penetration level, a higher TIS value obtained when lakes were short and thick rather than when they were thin and extended.

Going further in experimental observations to identify and validate tendencies would require many more samples to study and a more complete data set for each graft to help the comparison of the different tissues (such as an evaluation of the endothelial pump efficiency for example). Nonetheless, the next part of this paper is dedicated to the attempt to study and to numerically evaluate the influence of the different structural parameters aforementioned on the scattered light's intensity level.

#163673 - $15.00 USD Received 27 Feb 2012; revised 31 Mar 2012; accepted 29 Apr 2012; published 2 Jul 2012

3. Electromagnetic model for numerical simulations

To quantitatively link the structures observed in the samples with their measured scattering behavior, we used an electromagnetic vectorial theory developed previously for the study of low-scattering media [18,19]. The cornea, being transparent and presenting a relatively low scattering and weak refractive index mismatches, appears as a medium for which this theory may be applied, at least for reasonable edema states. OCT imagery gives access to local refractive index variations. Those images were then used as a tissue modelization to calculate the theoretical related far-field scattering intensity, and to compare it with the experimental measurements in order to explain the variations observed when the cornea swells.

The following paragraphs present a short recall of the theory we used, before establishing the limits in within which it was relevant to compare experimental and calculated data. The obtained numerical results are then presented in part 4.

3.1 First-order calculation method

This theory based on Born approximation [20] allows the calculation of the scattered field in both reflected and transmitted spaces for a stack of layers including rough interfaces and/or bulk heterogeneities. The method aims at solving the electromagnetic equations in the stack with weak inhomogeneity hypotheses:

$$\left|\frac{R_q}{\lambda}\right| \ll 1 \text{ and } |p| \ll 1$$

where R_q is the quadratic roughness of the considered interface in the case of surface scattering, and p the relative permittivity heterogeneity in the case of bulk scattering (full theory developments are presented in [19]). This parameter p is defined as

$$p = \frac{\Delta\varepsilon}{\varepsilon_{mean}}$$

with ε_{mean} the mean permittivity and $\Delta\varepsilon$ the local permittivity variation at every point inside the considered layer. Consequently, the permittivity for each point M within the layer can be written as follows:

$$\varepsilon_{(M)} = \varepsilon_{mean}\left[1 + p_{(M)}\right].$$

The resolution is carried out in two steps, the first one consisting in the calculation of the field as if the stack were perfect (i.e. a totally homogeneous medium without surface roughness) when it is illuminated with a monochromatic plane wave. This ideal field is supposed to be the only excitation source in the perturbed stack, and the scattered field is then calculated sequentially using the admittance method, taking into account the Fourier transform of the profile, or of the refractive index distribution.

The resulting intensity as a function of the scattering angle θ in the observation space may then be written as follows:

$$I(\theta) = \frac{4\pi^2}{S}\frac{\left|\mathbf{E}^d\right|^2}{\left|\mathbf{E}_0\right|^2}\frac{|\mathbf{k}|^3}{|\mathbf{k}_0|}\frac{\cos^2(\theta)}{\cos(i_0)}$$

where S is the illuminated surface of the sample, $\mathbf{E}_0$ and $\mathbf{k}_0$ the field and the wave vector in the incident medium, i_0 the incidence angle, $\mathbf{E}^d$ and $\mathbf{k}$ the field and the wave vector in the medium where the intensity I is measured. This intensity is calculated with respect to the polarization of the incident and scattered waves.

#163673 - $15.00 USD Received 27 Feb 2012; revised 31 Mar 2012; accepted 29 Apr 2012; published 2 Jul 2012

As we suppose no interaction between the different heterogeneities (simple scattering regime), the total field results in the addition of the contributions of the different scattering sources (originated from all the heterogeneous layers and rough interfaces of the stack).

The calculations are made for stacks whose description includes the number of layers, their thickness and mean refractive index, at one wavelength with a given incidence. The perturbation can be described in two or three dimensions for the different interfaces or layers, giving respectively the profile of the surface or the refractive index distribution within the layer. The method has the advantage of ensuring fast calculations without *a priori* thickness limitation.

3.2 Optical bandwidth

OCT imagery provides a micrometric resolved distribution of the structure in the cornea. We aimed to use these images as layer descriptions for numeric calculations of scattering intensity, and comparing these with the experimental far-field measurements to observe the different influences existing.

However, the potentiality of comparison between those two intensities (calculated vs. measured) must be ensured as the scale of the defects resolved by the different measuring devices may be different. To do so, we need to know the frequency domain (or optical bandwidth) available for each. Comparison is relevant only if it occurs on a same frequency bandwidth [21].

Plane wave formalism:

$$\mathbf{E} = \mathbf{E}_0 e^{-i\mathbf{k}.\mathbf{u}} e^{-i\omega t}$$

$$= \mathbf{E}_0 e^{-i(\alpha z + \boldsymbol{\sigma}.\mathbf{r})} e^{-i\omega t}$$

$$\mathbf{u} = (\mathbf{r}, z) = (x, y, z)$$

$$\mathbf{k} = (\boldsymbol{\sigma}, \alpha)$$

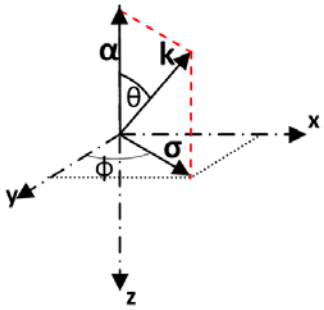

Fig. 10. Wave propagation vectors configuration.

Far-field scattering measurement selects only propagative scattered waves. Using the notations of Fig. 10, with a wave propagating in the z direction, all the waves with a real α component will be measured. As $\alpha = [k^2 - \sigma^2]^{½}$, with $k = 2\pi n/\lambda$ the wave vector and $\sigma/2\pi = n.\sin(\theta)/\lambda$ the spatial frequency for the scattering angle θ associated with the wave, it means that all the σ between 0 and k are eligible. As a consequence, scattering measurement in the reflected half-space at a wavelength λ implies an optical window in the domain $[2\pi n.\sin(\theta_{min})/\lambda ; 2\pi n.\sin(\theta_{max})/\lambda]$, where n is the refractive index of the observation medium and $[\theta_{min} ; \theta_{max}]$ is the measured angular range. With such an angular range between 20 and 90°, the bandwidth is included in the range [0.0034; 0.0099] nm^{-1}.

On the other hand, OCT imagery gives access to an image whose Fourier transform is sampled with a sampling rate of 2π/L (where L is the physical length of the observation window) to respect the Shannon theorem. As a consequence, supposing N the number of pixels in the image, we have access to a spatial frequency bandwidth of [0; 2πN/L]. Considering the device characteristics, we obtain a window in the range [0; 0.0083] nm^{-1}.

It appears both devices had a common frequency band: relevant comparison was then possible for scattering angles inferior to 56°, upper angles corresponding to image interpolation occurring in the calculation from the OCT image and *a priori* not representative of the real structure of the sample.

#163673 - $15.00 USD Received 27 Feb 2012; revised 31 Mar 2012; accepted 29 Apr 2012; published 2 Jul 2012

4. Model parameters and effects on scattering levels

This part is dedicated to numerical calculation results obtained with first-order approximation. However, the cornea being a highly complex sample in comparison with the thin-film multilayer configurations for which the theory was developed, we needed to define a simplified medium to represent it. As already announced, OCT images were to be used for the cornea modelization. This involved that only heterogeneities larger than one micrometer were to be taken into account in the calculations.

Hypotheses and simplifications adopted in order to model the cornea are first presented, before testing different parameters and finding out their possible influence on the scattering level.

4.1 Sample modelization

The representation of the cornea for electromagnetic calculations required to define firstly how to simplify the structure of the tissue, to keep only the elements appearing necessary to study the particular problem of the edema development influence over the scattering behavior. After introducing these simplifications, we describe which parameters were chosen and how they were applied to effectively run the simulations.

4.1.1 Corneal structural simplifications

For simplification purposes and according to the experimental observations, the choice was made to take into account only the stroma for the calculations: its thickness is predominant in the cornea and its structure is the most perturbed by edema development.

Furthermore we studied bulk scattering only, and no surface effect was taken into account. As observed experimentally, only angles inferior to 20° were influenced by the interface state of the sample so those angles were not considered. After introducing the parameters necessary to run bulk modeling calculations, we justify this choice by comparing the intensity levels related to bulk and surface scattering in Section 4.1.4.

4.1.2 OCT images processing

OCT images were used as heterogeneity distributions to describe the layers' bulk properties. Only those presenting no artifacts or parasites such as dust floating within the immersion liquid (BSS) were chosen. Moreover, to ensure *a minima* comparison between different samples' images, the greyscale of each was divided by the integration time used for the acquisition, and grey level values corresponding to the BSS on both side of the sample were adjusted to minimize the depth-induced signal loss due to the system.

The calculation requires a layer description in terms of relative permittivity inhomogeneity cartography. However, OCT images provide reflectance distributions, and are quantitatively related to the local refractive index mismatch strictly speaking. We made the choice to interpret those images only as structural cartographies of the stroma, and a refractive index scale we specify in the next paragraph was applied. Finally, once the stromal image is converted in a refractive index distribution $n(x,y,z)$, given that $\varepsilon = n^2$, we can convert it in relative permittivity inhomogeneity layer using the relation $p = 2\Delta n/n_{mean,}$ where Δn is the local refractive index mismatch relatively to the mean refractive index n_{mean} in the layer. The other parameters needed for computation are relative to the incident light (incidence angle, wavelength and polarization).

4.1.3 Refractive index parameters

As previously mentioned, the layer must be defined in term of refractive index distribution and it is also necessary to indicate its average refractive index. This one was set with the value $n_{mean} = 1.376$, corresponding to the mean refractive index of the cornea in physiological conditions [22]. As the properties of BSS are close to the ones of the aqueous humor, we

#163673 - $15.00 USD Received 27 Feb 2012; revised 31 Mar 2012; accepted 29 Apr 2012; published 2 Jul 2012

supposed this value remains realistic at least for thin corneas. We applied to the OCT images refractive index values scaled within the range $n_{mean} \pm \Delta n$, with Δn an amplitude to be determined.

We chose to consider as a reference the case of a transparent thin corneal graft (620 µm), such tissue being likely to complete conditions to fit the first-order hypothesis. Figure 11 presents the results obtained for different values of Δn, and the curves are compared with the experimental scattered intensity level measured for that cornea. The value of $\Delta n = 0.0025$ allowed both curves to match over the angular range of interest.

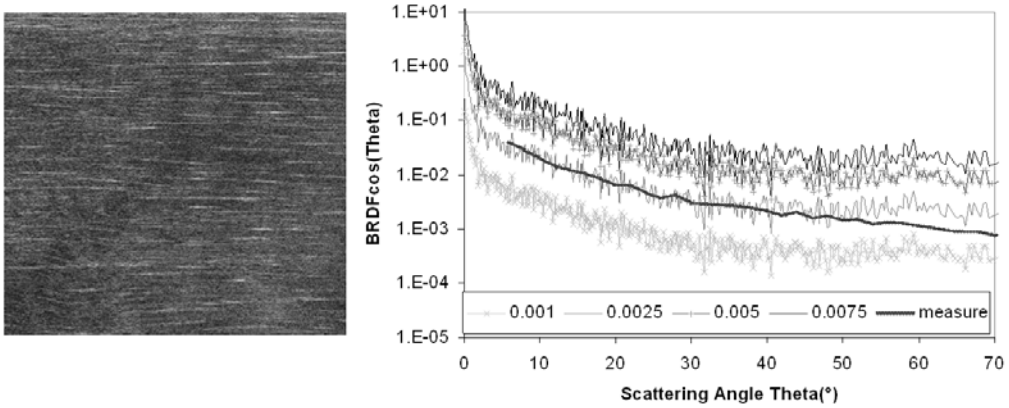

Fig. 11. Stroma OCT image used as a layer description (left) and refractive index amplitude Δn effect over scattering intensity from 620µm-thick sample (right) (simulations for $\Delta n = 0.001$, 0.0025, 0.005, 0.0075).

Having fixed this value Δn of refractive index amplitude, we tested the influence of the n_{mean} value over the calculated scattering intensity. Indeed, when the cornea swells, this supposes higher hydration and involves a modification of the average refractive index [23]. Nonetheless, we observe on Fig. 12 that this parameter's fluctuation is negligible in comparison to the Δn variation, as we obtained equivalent intensity levels whatever the value of n_{mean} between 1.33 and 1.4. As a consequence, the value of 1.376 was kept for the next simulations. For the same reason, the refractive index gradient within the stroma, inducing a higher average refractive index in the anterior part of the stroma rather than in the posterior part [22], was also neglected.

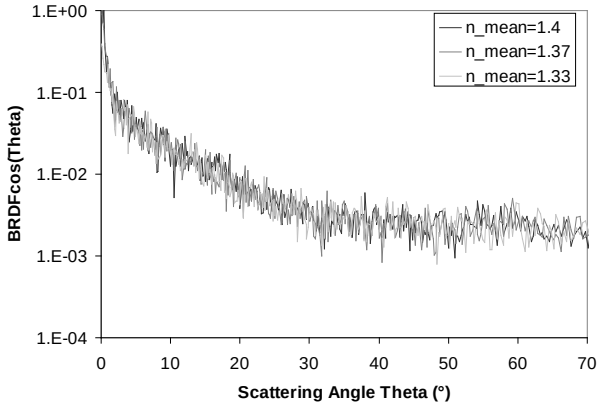

Fig. 12. n_{mean} influence over scattering level for the fixed refractive index amplitude $\Delta n = 0.0025$. The TIS variation depending on the value of n_{mean} from 1.33 to 1.4 is inferior to 2%.

#163673 - $15.00 USD Received 27 Feb 2012; revised 31 Mar 2012; accepted 29 Apr 2012; published 2 Jul 2012

4.1.4 Minor surface influence confirmation

We present here the calculations made to justify we didn't take into account the surface effect. We extracted two profiles from the OCT images, corresponding to the surfaces first of the epithelium, then of the Bowman's membrane (Fig. 13).

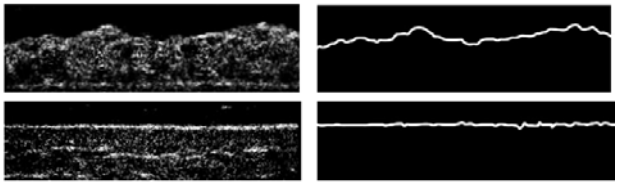

Fig. 13. Surface profiles extraction: Epithelium (up) and Bowman's membrane (down).

The calculated quadratic roughnesses were respectively 2.7 µm and. 0.35 µm. These values did not fit with the first-order approximation, so we solved the electromagnetic equations rigorously using a differential method based on an S-matrix algorithm [24,25].

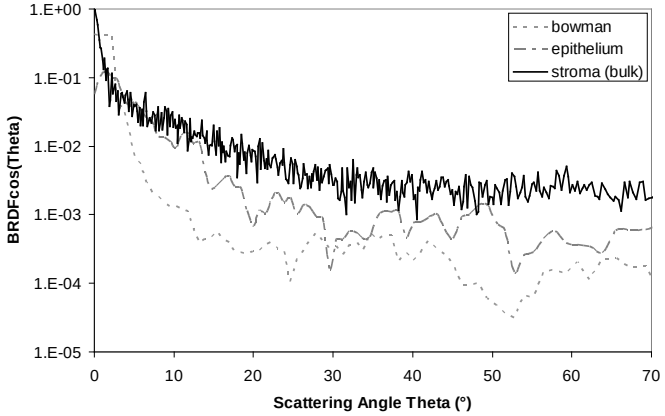

Fig. 14. Surface effect simulations for epithelium and Bowman's membrane surfaces and comparison with purely bulk scattered intensity level for a 620µm thick sample.

Figure 14 presents the superimposition of both surface calculations with the intensity level obtained for a 620 µm-thick sample considering a refractive index perturbation as described in the previous paragraph. We observe a major bulk influence, except in the low angles where surface effect has a greater impact. Nonetheless, those influences appear outside of the angular range of interest.

4.2 Structural influences

Having defined how the corneal grafts were to be modelized for calculations, several structural parameters were tested in order to interpret the experimental results. As observed experimentally, scattering level increases roughly with the thickness. Besides, both parameters do not present a simple relationship between them. Moreover, different structural organizations have been imaged while the edema develops. This paragraph aims at studying separately the influences of the thickness and of the structure over the scattering intensity.

4.2.1 Thickness

When studying the behavior of one graft, it appeared that the scattering level increased with the thickness. But although the trend was globally the same when comparing several tissues, the relationship was rougher. To study numerically the influence of the thickness, we firstly artificially increased the thickness of the reference sample, keeping the same density of

#163673 - $15.00 USD Received 27 Feb 2012; revised 31 Mar 2012; accepted 29 Apr 2012; published 2 Jul 2012

heterogeneities all along its depth (that would be equivalent to artificially adding extra tissue mass). Figure 15(a) shows the scattering levels obtained for thicknesses from 620 to 1200 µm, and we observe a limited increase, clearly inferior to the one obtained experimentally. If we calculate the TIS values over the angular range [20; 50°] and consider the ratio between the 620 µm and 1200 µm-thick samples, it is more than twice inferior to the same ratio calculated from the experimental measurements.

If the sample is now extended in the z direction (homogeneous dilation along the depth axis of the graft), the increase with thickness is much more significant as shown on Fig. 15(b).

Furthermore, if the TIS are calculated, we observe a parallel evolution of TIS and thickness in good agreement with the one obtained with experimental measurements for a

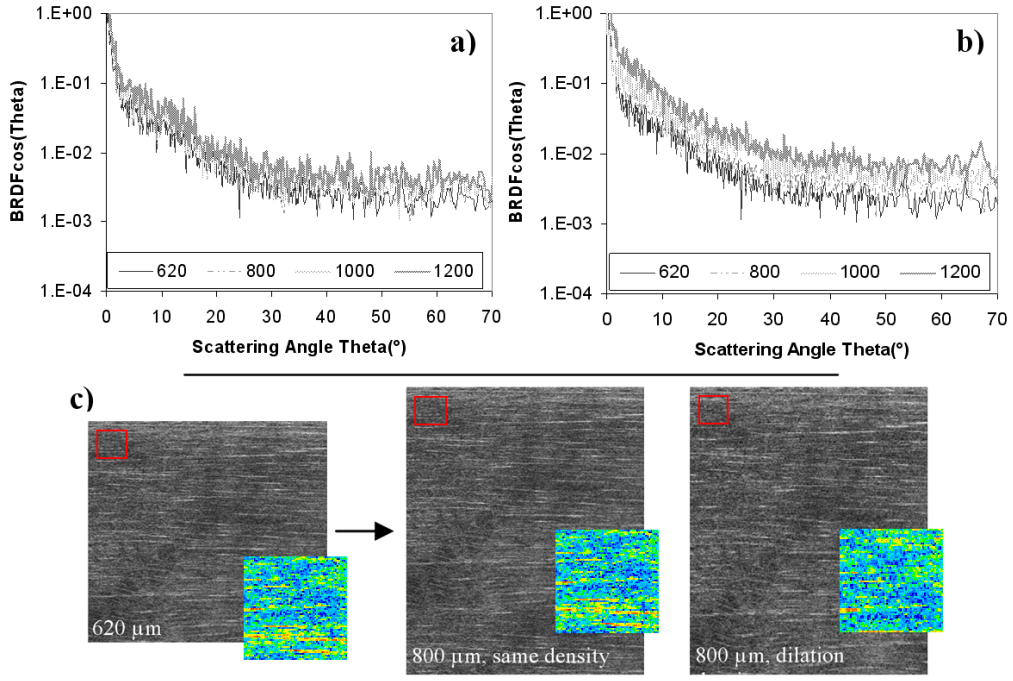

Fig. 15. Scattering intensity levels for different thicknesses with preserved (a) and z-dilated (b) microstructure repartitions within the layer. The image transformations are illustrated in (c) with zoom on equivalent areas on each image for comparison (false-color representation is used to highlight the structure's density differences).

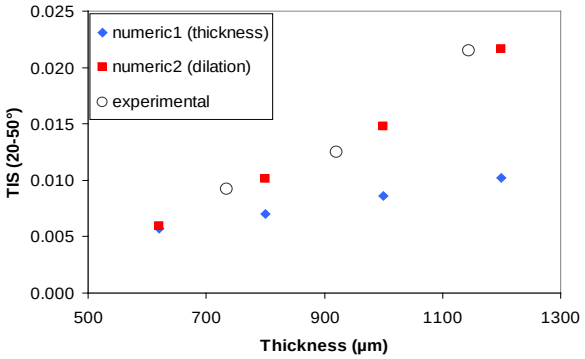

Fig. 16. TIS values plotted relatively to thickness. Comparison between experimental values for one cornea at different hydration states and two numeric simulations (thickness influence only and dilation effect).

#163673 - $15.00 USD Received 27 Feb 2012; revised 31 Mar 2012; accepted 29 Apr 2012; published 2 Jul 2012

cornea at different swelling states (Fig. 16). Although dilation following the z axis is a simplistic way to describe how a sample swells, it enlightens the importance of the structure's microscopic distribution, as thickness in itself does not totally explain the observed evolution of scattering.

4.2.2 Lakes distribution

We then tried to evaluate the influence of the lakes' distribution in the stroma. We could observe on the OCT images two distinct lake distributions, the first one including densely disposed thin wide lakes, and the second one with less extended thicker lakes, less numerous and sparsely distributed, as shown previously in Fig. 6.

To take into account the lakes' distribution only, we used a binary representation of the stroma, assuming a refractive index of 1.33 for the lakes, and 1.376 for the surrounding matrix. This induced a higher scattering level because of a more important refractive index mismatch. As a consequence, no direct comparison would be possible with the previous calculations and measurements.

OCT images were used to extract one lake's shape and localize the lakes' positions, considering the case of two grafts with similar thicknesses and equivalent lakes' penetration in the depth of the tissue. For both configurations, we calculated the TIS values, and compared the ratio of results relative to each distribution with the ratio of the corresponding experimental measurements.

TIS (20-50°)	Measurement	Calculus
Distribution 1 (D1)	0.02103	0.0519
Distribution 2 (D2)	0.01609	0.0412
D1/D2	1.3	1.26

Fig. 17. Binary models for lakes' distributions and TIS calculations compared with experimental values for 780 µm-thick corneas.

As summed up in Fig. 17, both experimental and numerical results enlightened a major scattering with the distribution involving short and thick lakes. Moreover, we obtained through measurements and calculations similar ratios highlighting the importance of the heterogeneity distribution's influence over the scattering intensity.

To conclude this paragraph, we have seen that thickness influence (extra-mass addition) on the scattering level of the layer is weak in comparison with the role of the structural repartition. But although structural evolution can't be reduced to a simple dilation, it appears that homogeneously spreading the heterogeneity along the depth of the sample leads to behaviors close to the experimental ones. Moreover, the shape and repartition of those heterogeneities is of great influence, and simulations give results in agreement with what has been experimentally observed.

4.3 Multi-sample study: consideration of higher thicknesses and scattering levels

While we previously considered the case of a thin and transparent cornea as a basis to study structural parameters, we then ran calculations for other samples, whose properties may question the use of the first-order approximation.

#163673 - $15.00 USD Received 27 Feb 2012; revised 31 Mar 2012; accepted 29 Apr 2012; published 2 Jul 2012

We considered several OCT images corresponding to different grafts, with different thicknesses and transparency states. We calculated the scattering intensity levels using the values of $\Delta n = 0.0025$ and $n_{mean} = 1.376$. We observed that the simulated levels fit the experimental curves while the graft remains thin with a clear appearance, but for higher thicknesses and cloudy states, the intensity is obviously under-evaluated in comparison with the experimental measurements (Fig. 18).

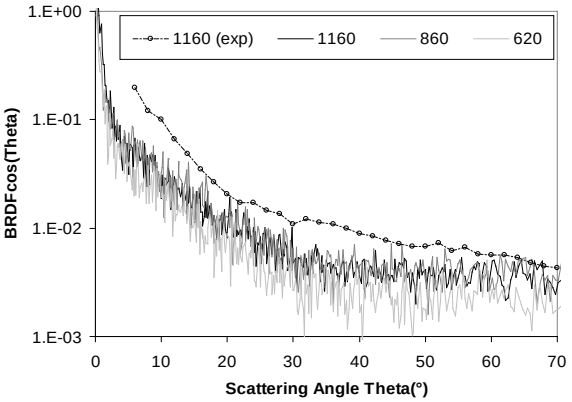

Fig. 18. Scattering levels calculated from OCT images of different grafts with several thicknesses and transparency states, applying $\Delta n = 0.0025$ and $n_{mean} = 1.376$; the experimental level for the thickest cornea is also indicated.

To explain these differences, it is necessary to define the limitations of the modeling. We do not come back here on the choice of the refractive index scale, but try to point out the hypothesis explaining why a combination of thickness and structure repartition is not sufficient to match experimental behaviors.

First of all, the numerical representation of the layers was limited to an enlightenment surface of 250x190 μm^2, which is little in comparison with the 1mm radius of the laser beam used to probe the graft experimentally. Therefore, all the existing structures were not taken into account and the numerical calculation does not benefit from the averaging effect occurring during the measure. Secondly, OCT images do not resolve structures smaller than less than one micrometer large. Finally, the choice of the Δn value was made considering a clear cornea, inducing low scattering. It is not surprising this parameter is underestimated when scattering increases, as the hypothesis of a single scattering regime may not be

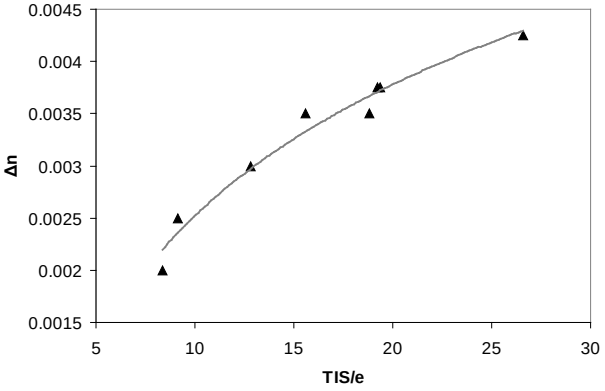

Fig. 19. Calculation of the Δn parameter matching experimental and calculated scattering levels in function of the parameter 10^{6}·TIS/e where e is the graft thickness and TIS is calculated on the range 20-50° from the experimental data.

#163673 - $15.00 USD Received 27 Feb 2012; revised 31 Mar 2012; accepted 29 Apr 2012; published 2 Jul 2012

reasonable anymore, while first-order approximation precisely does not take into consideration multi-scattering regimes.

To go further, we then calculated the values of Δn necessary to match experimental and calculated intensity levels for the different samples previously considered. We obtained that this parameter evolves with the experimental TIS value divided by the graft's thickness (we will denote this quantity TIS/e from now on; Fig. 19).

TIS/e may be understood as a linear scattering potential of the sample, analogically with the scattering coefficient μ_s, although we consider here a global behavior in the reflected half-space but the specular directions. The Δn parameter therefore appears as a corrective value related to TIS/e, figuring out the offset existing between the sample behavior and a first-order scattering reference behavior, quantifying the effects due to multi-scattering in particular.

5. Conclusion

This paper presents results obtained as a primary approach to achieve a characterization of the cornea in terms of transparency and scattering properties when an edema develops, with the possibility to extend it to *in vivo* diagnosis, which supposes a limitation to the reflective half-space. The study presented here focuses on human corneal grafts and their behavior when swelling, through the combination of the observation of their microscopic structure using OCT imagery, and of the far-field backscattered intensity measurement. First-order approximation modeling was then used to numerically link both aspects.

The experimental part of this study highlights two main aspects:

- The first one is related to scattering measurements in the reflective half-space, which enlighten preferential angular domains where a bulk origin appears as predominant for scattering. This allows the consideration of the Total Integration Scattering to quantify the scattering behavior of the sample, whose evolution correlates with the evolution of the thickness and transparency appearance. Its potential as metric should be confirmed through further studies including measurements in the transmitted half-space.

- Second, the microscopic imagery of the edematous grafts permits the observation within the stroma of the "lakes", which adopt two main repartitions depending on the graft considered, without any evident link with its thickness or opacity. Some grafts present preferentially long and thin lakes with an important density while more compact lakes are sparsely distributed in other tissues, leading to higher scattering intensity levels than in the first case. This highlights the role of micrometric structures over the scattering when the cornea swells.

The use of electromagnetic modeling based on first-order approximation, with respect to a simplified representation of the samples, gives results in accordance with the experimental behavior observed when considering the importance of the structural repartition inside the bulk. Furthermore, the modeling enables a numerical link between the grafts' structural and scattering properties through the relationship between the parameters Δn and TIS/e, as presented on Fig. 19.

To conclude, a characterization of the edematous state of a corneal graft therefore appears already achievable, although a simple representation of the tissue which requires improvements: a more complete description of the tissue in the modeling, the correct determination of the refractive index repartition within the tissue, and also a calibration of the method, studying on the one hand phantoms with controlled properties -to be able to determine representative parameters of the layer heterogeneity from the scattering level-, and on the other hand more corneal grafts, in particular tissues eligible for transplant, with the view to offer a new tool for graft sorting.

#163673 - $15.00 USD Received 27 Feb 2012; revised 31 Mar 2012; accepted 29 Apr 2012; published 2 Jul 2012

Acknowledgments

The authors thank Dr. Nouaille de Gorce and the tissue bank service of the Etablissement Français du Sang de Marseille for providing the grafts necessary for the study, and Pr. Patrick Fournier for English correction.

#163673 - $15.00 USD Received 27 Feb 2012; revised 31 Mar 2012; accepted 29 Apr 2012; published 2 Jul 2012